Importance of recent shifts in soil thermal dynamics on growing season length, productivity, and carbon sequestration in terrestrial high-latitude ecosystems

E. S. EUSKIRCHEN*, A. D. McGUIRE†, D. W. KICKLIGHTER‡, Q. ZHUANG§, J. S. CLEIN*, R. J. DARGAVILLE¶, D. G. DYE‖, J. S. KIMBALL**, K. C. McDONALD††, J. M. MELILLO‡, V. E. ROMANOVSKY‡‡ and N. V. SMITH§§

*Institute of Arctic Biology, University of Alaska Fairbanks, Fairbanks, AK 99775, USA, †US Geological Survey, Alaska Cooperative Fish and Wildlife Research Unit, University of Alaska Fairbanks, Fairbanks, AK 99775, USA, ‡The Ecosystems Center, Marine Biological Laboratory, Woods Hole, MA 02543, USA, §Departments of Earth and Atmospheric Sciences and Agronomy, Purdue University, West Lafayette, IN 47907, USA, ¶CLIMPACT, Université Pierre et Marie Curie, 75252 Paris Cedex 05, France, ‖Frontier Research Center for Global Change, Japan Agency for Marine-Earth Science and Technology, Yokohama, Japan, **Flathead Lake Biological Station, Division of Biological Sciences, The University of Montana, Polson, MT 59860, USA, ††Jet Propulsion Laboratory, California Institute of Technology, Pasadena, CA 91101, USA, ‡‡Geophysical Institute, University of Alaska Fairbanks, Fairbanks, AK 99775, USA, §§Geological and Planetary Sciences and Environmental Science and Engineering, California Institute of Technology, Pasadena, CA 91125, USA

Abstract

In terrestrial high-latitude regions, observations indicate recent changes in snow cover, permafrost, and soil freeze–thaw transitions due to climate change. These modifications may result in temporal shifts in the growing season and the associated rates of terrestrial productivity. Changes in productivity will influence the ability of these ecosystems to sequester atmospheric CO_2. We use the terrestrial ecosystem model (TEM), which simulates the soil thermal regime, in addition to terrestrial carbon (C), nitrogen and water dynamics, to explore these issues over the years 1960–2100 in extratropical regions (30–90°N). Our model simulations show decreases in snow cover and permafrost stability from 1960 to 2100. Decreases in snow cover agree well with National Oceanic and Atmospheric Administration satellite observations collected between the years 1972 and 2000, with Pearson rank correlation coefficients between 0.58 and 0.65. Model analyses also indicate a trend towards an earlier thaw date of frozen soils and the onset of the growing season in the spring by approximately 2–4 days from 1988 to 2000. Between 1988 and 2000, satellite records yield a slightly stronger trend in thaw and the onset of the growing season, averaging between 5 and 8 days earlier. In both, the TEM simulations and satellite records, trends in day of freeze in the autumn are weaker, such that overall increases in growing season length are due primarily to earlier thaw. Although regions with the longest snow cover duration displayed the greatest increase in growing season length, these regions maintained smaller increases in productivity and heterotrophic respiration than those regions with shorter duration of snow cover and less of an increase in growing season length. Concurrent with increases in growing season length, we found a reduction in soil C and increases in vegetation C, with greatest losses of soil C occurring in those areas with more vegetation, but simulations also suggest that this trend could reverse in the future. Our results reveal noteworthy changes in snow, permafrost, growing season length, productivity, and net C uptake, indicating that prediction of terrestrial C dynamics from one decade to the next will require that large-scale models adequately take into account the corresponding changes in soil thermal regimes.

Keywords: carbon sequestration, climate change, growing season, permafrost, productivity, respiration, snow cover, terrestrial ecosystem model

Received 13 July 2005; revised version received 28 September 2005; accepted 7 October 2005

Correspondence: E. S. Euskirchen, tel. 907 474 1958,
e-mail: ffese@uaf.edu

Introduction

In recent decades, the increase of greenhouse gases in the atmosphere has been implicated as a primary factor in rising surface air temperatures (IPCC, 2001). Associated with these rising air temperatures are changes in freeze–thaw regimes and a decrease in the amount and depth of sea ice (Hansen *et al.*, 2001). It has been suggested that these trends are stronger over some high-latitude regions (Chapman & Walsh, 1993; Serreze *et al.*, 2000; Hansen *et al.*, 2001), with northern regions expected to exhibit increases greater than 1.5–4.5 °C of the global mean by 2100 (IPCC, 2001). These climate-induced changes are expected to continue into the 21st century, altering snow cover, permafrost stability, growing season length, and productivity in arctic and boreal systems.

The growing season begins in the spring with increasing temperatures and light availability, the melting of snow, thawing of the soil organic horizons, and the onset of photosynthesis. In the fall, the growing season terminates as temperatures and light availability decrease, the soils refreeze, and photosynthesis ceases. Earlier thawing of the soils and later refreezing of the soils has also been associated with an increase in permafrost degradation (Osterkamp & Romanovsky, 1999; Poutou *et al.*, 2004; Sazonova *et al.*, 2004). Modifications in growing season length and permafrost stability can alter productivity and carbon (C) sequestration (Myneni *et al.*, 1997; Goulden *et al.*, 1998), possibly resulting in changes in the amplitude of the annual cycle of CO_2 (Keeling *et al.*, 1996; Randerson *et al.*, 1999). The implications of these recent and projected changes in terms of C uptake and release across high-latitude regions remain poorly understood.

Net ecosystem productivity (NEP) in terrestrial ecosystems depends on the difference between net primary productivity (NPP) and heterotrophic respiration (R_h), where positive values of NEP indicate a C sink, and negative values indicate a C source. NEP could increase or decrease in response to changes in soil freeze–thaw regimes, with increases likely due to enhanced productivity during a longer growing season. However, this enhanced productivity could be counter-balanced by increased respiration from soil heterotrophs. Northern soils contain large amounts of organic matter, and soil heterotrophs are generally more responsive in warm temperatures. Consequently, increases in soil temperature are associated with an increase in soil organic matter decomposition and increased available nutrient supplies. These increases may, in turn, lead to increased rates of photosynthesis (Van Cleve *et al.*, 1990), although any gains made in vegetation C due to increased available nutrient supplies can be offset by soil C losses

(Mack *et al.*, 2004). Areas with degrading permafrost would possibly exhibit high C losses due to increased amounts of respiration from these C-rich soils (Oechel & Billings, 1992).

Regional scale studies based on remote sensing data from high latitudes during the past two to three decades have found decreases in snow cover duration and extent (Dye, 2002; Dye & Tucker, 2003), changes in soil freeze–thaw regimes that result in either an earlier onset or shift of the growing season in high-latitude ecosystems (McDonald *et al.*, 2004; Smith *et al.*, 2004), and an increase in summer greenness, plant growth, and aboveground vegetation C (Myneni *et al.*, 1997, 2001; Zhou *et al.*, 2001). The recent availability of these spatially explicit data provides an opportunity to evaluate if a large-scale process-based model captures these changes in snow cover, soil freeze–thaw regimes, and growing season length. To our knowledge, models have not been evaluated with these spatially explicit data. Thus, the first question in our study is (1) How realistic are model simulations when evaluated against spatially explicit data? Furthermore, it is not clear what these changes might mean to terrestrial C dynamics, both above- and belowground. Therefore, the second question of this study is (2) What are the implications of recent observed changes in snow cover, soil freeze–thaw regimes, and the timing and length of the growing season on terrestrial C dynamics? Finally, observations are limited to past changes, whereas some process-based models can be used to explore the potential consequences of future global warming. Consequently, our third question is (3) What changes are likely to occur in the future with global warming?

Methods

Overview

We evaluated how changes in atmospheric CO_2 concentrations and climate may alter net C uptake in terrestrial high-latitude regions using the terrestrial ecosystem model (TEM, version 5.1). Following model calibration, we performed two types of model simulations that took into account: (1) retrospective transient climate and increases in CO_2 concentrations for the years 1960–2000, and (2) prognostic transient climate and increases in CO_2 concentrations for the years 2001–2100. We then calculated changes in snow cover, soil freeze–thaw, growing season length, permafrost distribution, and C dynamics over this 1960–2100 time period, and, when possible, validated our results with remotely sensed data. We examined these patterns over high-latitude land areas based on several different categories, including extra-tropical regions between

30–60°N and 60–90°N, continents, and snow classification regions.

TEM

The TEM is a process-based, global-scale ecosystem model that incorporates spatially explicit data pertaining to climate, vegetation, soil, and elevation to estimate monthly pools and fluxes of C and N in the terrestrial biosphere (Fig. 1). The underlying equations and parameters have been extensively documented (Raich et al., 1991; McGuire et al., 1992; Tian et al., 1999), and the model has been applied to a number of studies in high-latitude regions (e.g. Clein et al., 2000, 2002; McGuire et al., 2000a, b, 2002; Zhuang et al., 2002, 2003, 2004). In this study, we implemented TEM version 5.1, which is revised from TEM version 5.0 (Zhuang et al., 2003), with an updated freeze–thaw algorithm.

TEM 5.1 is coupled to a soil thermal model (STM; Zhuang et al., 2001) that is based on the Goodrich model (Goodrich, 1976) and takes a finite element approach to determining heat flow in soils (Fig. 1). This model is appropriate for both permafrost and non-permafrost soils. The STM receives monthly, gridded estimates of air temperature, soil moisture, and snowpack from TEM. The monthly snowpack estimates are a function of elevation, as well as monthly precipitation and monthly air temperature, and have a subsequent influence on soil moisture in the water balance model of TEM. Snowpack accumulates whenever mean monthly temperature is below −1 °C, and snowmelt occurs at or above −1 °C. Although it would seem intuitive for snow to melt at 0 °C, the value of −1 °C is used to account for the monthly time-step of TEM vs. the actual within month variations in air temperature that are slightly greater or less than 0 °C. At elevations of 500 m or less, the model removes the entire snowpack, plus any new snow by the end of the first month with temperatures above −1 °C. At elevations above 500 m, the melting process requires 2 months above −1 °C, with half of the first month's snowpack retained to melt during the second month (Vörösmarty et al., 1989).

The snowpack, air temperature, and soil moisture data are used in the STM to simulate soil temperatures at different depths such that the frozen and thawed boundaries in the soil move up and down during a simulation. Based on these soil temperatures, a sub-monthly freeze–thaw index is calculated to determine the day of the month that soils are frozen or thawed. This index is a proportion of the month in which the ground is thawed. It influences the ability of the vegetation to take up atmospheric CO_2 and is used as a multiplier in the calculation of gross primary productivity (GPP). A greater proportion of soil thaw leads to higher values of GPP while a smaller proportion of soil thaw yields lower values of GPP (Zhuang et al., 2003).

The freeze–thaw algorithm implemented in this study (Table 1) is based on a weighted running mean of soil temperature at a depth at 10 cm since previous analyses with TEM showed that the timing of thaw at this depth agreed well with the onset of photosynthesis for ecosystems above 30°N (Zhuang et al., 2003). The algorithm designed for this study was updated from Zhuang et al. (2003) in order to more adequately capture changes in soil temperature on freeze–thaw events. The weighted running mean incorporates soil temperatures from the previous month (T_{m-1}), current month (T_m), and next month (T_{m+1}; Table 1). The highest weights given to those months representing the transition from early or late spring to summer or the transition from late summer to autumn. The second highest weights are given to those months representing the transition from late winter to early spring or from late autumn to winter. Freeze–thaw events that are anomalous are given the lowest weights (Table 1).

Based on the combination of the frozen and non-frozen months, the day of thaw and day of freeze are calculated by first subtracting the proportion of the month that is thawed from the Julian day corresponding to the end of the particular month over which the thaw or freeze has occurred. Subtracting the day of freeze from the day of thaw yields the length of the annual non-frozen period, which is used as a surrogate for the growing season. The area of permafrost distribution is estimated based on the soil temperatures from 0 to 200 cm, where those areas with mean soil temperatures remaining below 0° C for two or more consecutive years are considered permanently frozen ground (Permafrost Subcommittee, 1988).

Model application

Input data sets

Contemporary data sets. Our monthly climate data for the years 1901–2000 pertaining to cloudiness (%), precipitation (mm), and air temperature (°C) were obtained from the Climate Research Unit database (CRU, Mitchell et al., 2004). The gridded soil texture data is based on the *Food and Agriculture Organization/ United Nations Educational Scientific and Cultural Organization (FAO/UNESCO)* [1974] soil map of the world. The input vegetation map is described in Melillo et al. (1993), and the input elevation map is based on 10 min digital global elevation data (NCAR/Navy, 1984). These climate, soil, vegetation, and elevation data sets are 0.5° latitude by 0.5° longitude resolution with land areas above 30°N represented by 40 424 grid cells. In addition, we obtained data pertaining to atmospheric
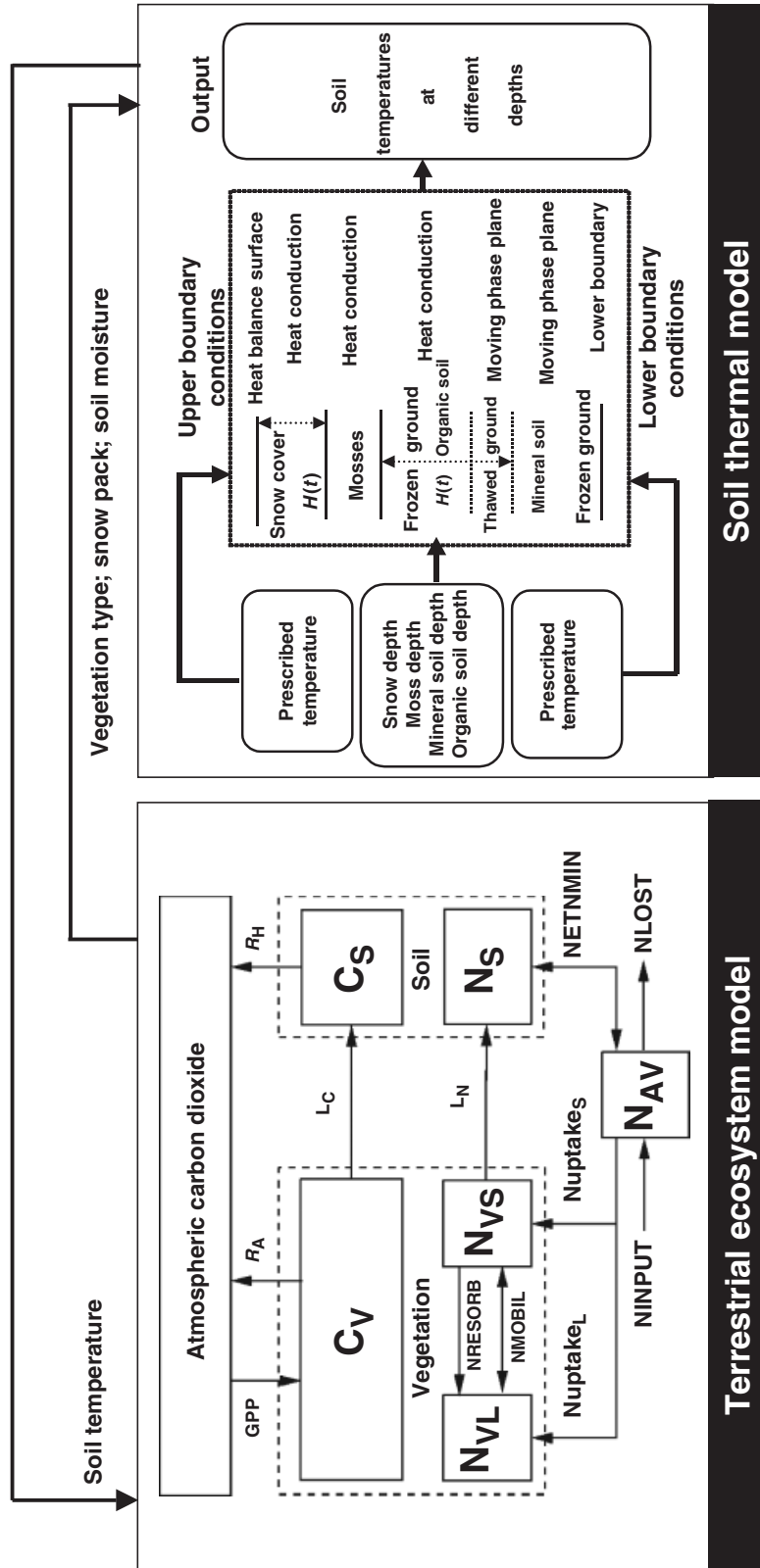
Fig. 1 Conceptual diagram of the terrestrial ecosystem model (TEM) coupled to the soil thermal model (STM).

Table 1 The weights of the running mean of monthly soil temperature (T_m; 10 cm depth) used to calculate the freeze–thaw index in TEM

T_{m-1}	T_m	T_{m+1}	Weight	Explanation
−	+	+	0.6	The transition from early or late spring to summer
+	+	−	0.6	The transition from late summer to autumn
−	−	+	0.5	The transition from late winter to early spring
+	−	−	0.5	The transition from late autumn to winter
−	+	−	0.3	Anomalous conditions
+	−	+	0.3	Anomalous conditions
+	+	+	No weight	The freeze–thaw index is set to '1'.
−	−	−	No weight	The freeze–thaw index is set to '0'.

T_{m-1} is the soil temperature of the previous month, T_m is the soil temperature of the current month, and T_{m+1} is the soil temperature of the next month, and a ' + ' indicates that the monthly mean temperature is above $0\,°C$ and a '−' indicates that the monthly mean temperature is below or equal to $0\,°C$.
TEM, terrestrial ecosystem model.

CO_2 with observations averaged from Mauna Loa and South Pole stations (Keeling *et al.*, 1995, updated).

Prognostic data sets. To generate the data sets for predictions of transient climate change for the 21st century, our overall methodology followed that of Xiao *et al.* (1997, 1998). This involved the use of the integrated global system model (IGSM) developed at the Massachusetts Institute of Technology (MIT), which is a 2-D land–ocean climate model that simulates the surface climate over the land and ocean for 23 latitudinal bands globally (Sokolov & Stone, 1998). The climate outputs during the years 1977–2100 from a 'reference scenario' by the MIT model (Webster *et al.*, 2003) were linearly interpolated to 0.5°-resolution bands, and the interpolated values subsequently applied to all grid cells within a 0.5°-latitudinal band.

To assemble the future climate, we overlay the projected changes in climate on the mean contemporary climate based on the period 1931–1960 from the CRU database. The absolute differences in mean monthly temperatures and the ratios in monthly precipitation and monthly mean cloudiness for 1977–2100 were then calculated, with the baseline values comprising the simulated climate data from the IGSM. The absolute differences in monthly mean temperature from 1977 to 2100 were then added to the contemporary monthly mean temperature data. Similarly, the ratios in monthly precipitation and monthly mean cloudiness from 1977 to 2100 were multiplied by the contemporary monthly precipitation and monthly mean cloudiness data, respectively. Given the large climate zones over which these values are interpolated, analyses with these data are best restricted to regional scales (Xiao *et al.*, 1997). To assess similarities and differences between the data sets, we compared the baseline 1977–2000 period of input climatic prognostic data to these same years of CRU data. We also compared output data for trends in snow, freeze–thaw and C dynamics based on TEM simulations incorporating the interpolated climate data set and the CRU data for the baseline period. The transient future input data pertaining to average global CO_2 concentrations was based on that of Keeling *et al.* (1995, updated), increasing from 372.02 ppm in 2001 to 690.93 ppm in 2100 in increments of $0.45–5.46\,\text{ppm yr}^{-1}$ (Xiao *et al.*, 1997).

Comparisons of the decadal means and standard deviations between the CRU data set and the interpolated climate data set from the IGSM for the regions between 30–60°N and 60–90°N during the baseline period of 1977–2000 generally showed good agreement between the two data sets (Table 2). From 1977 to 2000, mean annual air temperatures increased by $0.7\,°C$ in the CRU data set and by $0.5\,°C$ in the interpolated data set for the 30–60°N region. In the 60–90°N region, mean annual air temperature increased by $1.1\,°C$ in CRU data set and by $0.9\,°C$ in the interpolated data set. Total amounts of precipitation were greater based on the CRU data set than the interpolated data set, particularly within the 30–60°N region (Table 2). However, both data sets showed increases in precipitation by approximately 5 mm during the years 1977–2000. Comparisons of percent cloudiness differed between the CRU and interpolated data sets by ≤ 1% (Table 2).

The annual mean temperature in the 30–60°N region increased from $5.8\,°C$ during the years 2001–2010 to $9.0\,°C$ during 2090–2100 (Table 2). In the 60–90°N region, the air temperature increased from $-9.9\,°C$ during 2001–2010 to $-3.5\,°C$ during 2090–2100 (Table 2). These were increases ranging from approximately $0.2\,°C$ to $0.9\,°C$ per decade in both the 30–60°N and 60–90°N regions (Table 2). Precipitation also increased during the years 2001–2100. This increase was from a mean of

Table 2 Mean (SD) annual air temperature (T_{air}), mean (SD) total (SD) precipitation, and mean (SD) annual cloudiness based on the CRU data set and the prognostic data set

Data set	Years	T_{air} (°C)		Precipitation (mm)		Cloudiness (%)	
		30–60°N	60–90°N	30–60°N	60–90°N	30–60°N	60–90°N
CRU prognostic	1977–1980	5.2 (8.3)	−11.8 (8.4)	580.1 (381.7)	363.6 (242.0)	57.5 (16.6)	67.3 (11.4)
		5.1 (8.1)	−10.9 (8.2)	554.6 (360.5)	364.0 (241.4)	56.5 (15.4)	66.9 (9.5)
CRU prognostic	1980–1990	5.5 (8.2)	−11.3 (8.3)	581.6 (390.1)	371.0 (244.9)	56.8 (16.8)	66.5 (11.3)
		5.5 (8.1)	−10.5 (8.1)	559.2 (364.0)	365.3 (239.9)	57.2 (15.4)	67.3 (9.8)
CRU prognostic	1990–2000	5.9 (8.2)	−10.9 (8.2)	583.9 (396.2)	368.6 (244.0)	56.3 (16.8)	66.7 (11.0)
		5.6 (8.1)	−10.1 (8.2)	560.8 (364.8)	368.5 (242.5)	56.9 (15.5)	67.2 (9.8)
	2000–2010	5.8 (8.0)	−9.9 (8.4)	557.4 (362.3)	369.5 (244.1)	56.4 (15.4)	67.2 (9.8)
	2010–2020	6.1 (8.0)	−9.2 (8.5)	560.5 (364.8)	374.4 (247.5)	56.1 (15.4)	67.2 (9.7)
	2020–2030	6.6 (7.9)	−8.5 (8.7)	566.1 (368.1)	381.2 (253.0)	56.4 (15.5)	67.7 (9.8)
	2030–2040	6.8 (7.9)	−7.9 (8.6)	567.0 (368.1)	381.9 (254.3)	56.4 (15.8)	66.9 (9.9)
Prognostic	2040–2050	7.1 (7.9)	−7.5 (8.5)	569.9 (370.3)	391.0 (260.3)	56.6 (16.2)	68.7 (10.3)
	2050–2060	7.3 (7.9)	−7.2 (8.5)	571.8 (371.2)	391.4 (261.1)	56.6 (16.3)	68.2 (10.4)
	2060–2070	7.6 (7.9)	−6.1 (8.7)	575.7 (374.6)	397.2 (265.2)	56.8 (16.4)	69.1 (10.5)
	2070–2080	8.0 (7.9)	−5.2 (8.8)	581.5 (376.5)	409.5 (272.4)	56.9 (16.6)	69.6 (10.7)
	2080–2090	8.5 (7.8)	−4.4 (8.8)	587.6 (379.8)	416.0 (276.3)	57.2 (16.8)	70.9 (11.0)
	2090–2100	9.0 (7.8)	−3.5 (8.8)	597.8 (385.1)	423.4 (281.1)	57.2 (16.8)	70.7 (10.8)

The baseline period of 1977–2000 is shown to compare the CRU data with the interpolated data set used in the prognostic simulations (referred to as 'prognostic').

CRU, Climate Research Unit; SD, standard deviation.

557 mm mean during 2000–2010 to 598 mm during 2090–2100 in the 30–60°N region. In the 60–90°N region, this increase was from a mean 370 mm during 2000–2010 to 423 mm during 2090–2100. Between 2001 and 2100, percent cloudiness increased by <1% in the 30–60°N region and by 3.5% in the 60–90°N region.

Model calibrations. Many of the parameters in TEM are defined from published values in peer-reviewed literature. However, the rate limiting parameters are determined by calibrating the model to the pools and fluxes of intensively studied field sites that are representative of those in a particular region. For this study, we followed a calibration procedure described by Zhuang *et al.* (2003), which includes estimating rate limiting parameters for GPP, autotrophic respiration (R_a), R_h, plant nitrogen uptake, and soil nitrogen immobilization for sites representing seven vegetation types (see Table 2 of Zhuang *et al.*, 2003). There is no rate limiting parameter for gross nitrogen mineralization as it is tightly coupled to R_h through the C:N ratio of soil organic matter.

Model simulations. We conducted two TEM simulations, consisting of: (1) a retrospective analysis, with transient phases of both climate and CO_2 concentrations for the years 1960–2000, and (2) a prognostic simulation with transient phases of climate and CO_2 concentrations for the years 2000–2100. To initialize the retrospective

simulations, we ran TEM to equilibrium for all grid cells north of 30°N following the protocol of Zhuang *et al.* (2003), which consisted of using the mean climate from 1901 to 1930, as the equilibrium in 1900 (Mitchell *et al.*, 2004). We then ran the model from 1900 to 2000, and analyzed model output for the years 1960–2000. The equilibrium pools of C and N estimated for this climate were used as the initial conditions for the simulation. The model was initialized with the atmospheric concentration of CO_2 in year 1901, which was 296.3 ppm. To initialize the prognostic simulations we followed the protocol of Xiao *et al.* (1997, 1998) by running TEM to equilibrium for all grid cells north of 30°N, using the mean climate from 1977 to 2000 as the equilibrium climate in 1976, and the atmospheric concentration of CO_2 in year 1976, which was 337.3 ppm. The equilibrium pools of C and N estimated for this climate were used as the initial conditions for simulations from 1976 to 2100. We analyzed future conditions using the years 2000–2100 from the model output.

Model evaluation

Snow cover, soil freeze–thaw, and growing season length comparisons. To examine the effects of increasing CO_2 concentrations and temperature on snow cover and soil freeze–thaw regimes, we compared our simulated seasonal dynamics of snow cover, soil freeze–thaw, and growing season length to those based on remote sensing studies. For the snow cover evaluation, we

compared our simulations with the satellite-based analyses for the period 1972–2000 by Dye (2002). We analyzed three patterns of regional snow cover across the entire TEM data set and the entire data set of Dye (2002), using regional classifications similar to Dye (2002). This included grouping regions based on the month of first snow (MFS), month of last snow (MLS), and duration of snow-free (DSF) period, with each of these three classifications containing three subgroups. Regions defined by the MFS classification were those with the month of first continuous snow occurring in September (MFS-Sep), October (MFS-Oct), or November (MFS-Nov). Within the MLS region, areas were grouped depending on when the month of last continuous snow cover occurred: April (MLS-Apr), May (MLS-May), or June (MLS-Jun). The regions for the DSF classification were based on the length of continuous snow free period occurring for 8–18 weeks (DSF-R1), 18–28 weeks (DSF-R2), or 28–37 weeks (DSF-R3). As further validation of the snowmelt variable output from our model, we examined the annual values of the duration of the snow free period for each of the DSF regions of the TEM and Dye (2002) data sets. To reduce bias in these comparisons, we only used grid cells with available data across both data sets, and did not attempt to fill data gaps.

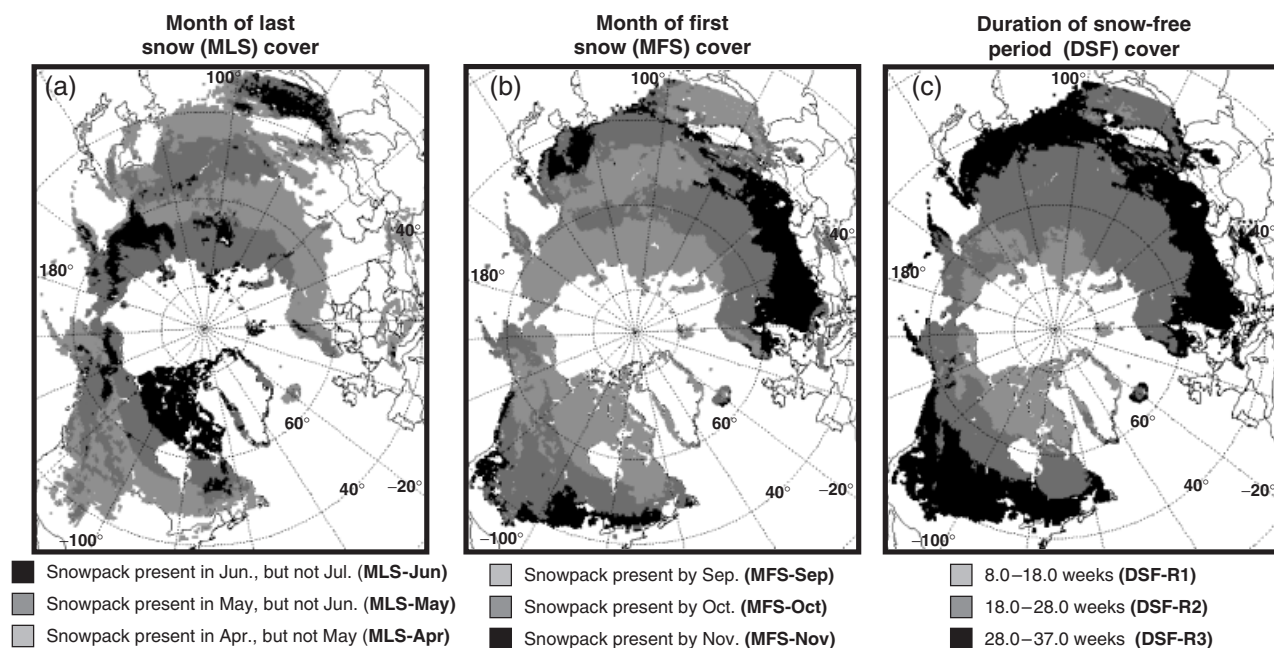Our evaluation of soil freeze–thaw and growing season length anomalies incorporated two studies of land-surface thaw based on the special sensor microwave/imager (SSM/I) satellite data. Both studies encompassed the same period, 1988–2000, but used different data-processing algorithms (McDonald et al., 2004; Smith et al., 2004). Consequently, the study of McDonald et al. (2004) focused solely on thaw date in the spring while that by Smith et al. (2004) calculated both a date of thaw and date of freeze, and subtracted the date of freeze from the date of thaw to estimate growing season length. As above, in this analysis we only used grid cells with available data across all three data sets, and did not fill gaps.

We compared our estimate of the southern permafrost boundary with that of the Circum-Arctic permafrost map from Brown et al. (1998, revised 2001). This map depicts the permafrost extent in terms of continuous (90–100%), discontinuous (50–90%), sporadic (10–50%), and isolated patches (0–10%) for the Northern Hemisphere, encompassing the area between 25–90°N and 180°W–180°E.

Results

Retrospective trends in snow cover, soil freeze–thaw, growing season length, and permafrost

Our overall patterns of snow cover across the three snow classification regions (Fig. 2) were in generally good agreement with that of Dye (2002) during the

Month of last snow (MLS) cover	Month of first snow (MFS) cover	Duration of snow-free period (DSF) cover
(a)	(b)	(c)

Snowpack present in Jun., but not Jul. (**MLS-Jun**)
Snowpack present in May, but not Jun. (**MLS-May**)
Snowpack present in Apr., but not May (**MLS-Apr**)

Snowpack present by Sep. (**MFS-Sep**)
Snowpack present by Oct. (**MFS-Oct**)
Snowpack present by Nov. (**MFS-Nov**)

8.0–18.0 weeks (**DSF-R1**)
18.0–28.0 weeks (**DSF-R2**)
28.0–37.0 weeks (**DSF-R3**)

Fig. 2 Geographical depiction of the snow cover regions derived from the mean values over the years 1972–2000 calculated from the retrospective simulation. In (a) the month of last snow (MLS) regions are based on the final month of continuous snowpack. In (b) the month of first snow (MSF) regions are based on the month of first continuous snowpack. In (c) the duration of snow free (DSF) period is calculated based on the number of weeks between the month of last snow cover and the month of first snow cover.

years 1972–2000, with Pearson rank correlation coefficients ranging from 0.58 to 0.65. Comparisons between the 'percent of total area' across the three snow classification regions showed that the data of Dye (2002) and TEM generally agreed by $\pm 14\%$, with most regions agreeing by $\pm 5\%$ (Table 3). On an interannual basis, the agreement between the TEM and Dye (2002) data sets for the duration of the snow free period (Fig. 3) indicated that the two studies were more highly correlated in the regions further south (DSF-R2 and DSF-R3; e.g. areas with greater forest cover) than the region further north (DSF-R1; e.g. areas of tundra). This discrepancy is potentially attributable to the accuracy of the input TEM data sets at high-latitudes where the instrumental climate data is scarce. Discrepancies between TEM and the Dye (2002) data might also be due to uncertainties associated with interpreting the remote sensing data. Factors that may reduce the reliability of remotely sensed snow cover data include low solar illumination and high solar zenith angles and cloud cover (Dye, 2002).

Taking into account all grid cells for the region north of 30°, the areas of the three snow classification regions decreased between 1960 and 2000, with trends similar to those estimated by Dye (2002). Based on the slopes of

the least-squares regressions for each region, this trend was the strongest in the MLS and DSF regions, with a total decrease of $12.8 \times 10^4 \, \text{km}^2 \, \text{yr}^{-1}$ in the MLS region, and $11.3 \times 10^4 \, \text{km}^2 \, \text{yr}^{-1}$ in the DSF region. The trend was weakest in the MFS region, with a total decrease of $6.6 \times 10^4 \, \text{km}^2 \, \text{yr}^{-1}$ (Table 4). Corresponding with these trends, examination of the monthly air temperatures of the input CRU data indicated that increases in air temperature were greater in the spring than the fall (Table 4).

The slopes of least-squares regression analysis for each grid cell also supplied an assessment of the rate of change in the annual anomalies of day of thaw, day of freeze, and growing season length. The data sets of McDonald *et al.* (2004), Smith *et al.* (2004), and that from TEM consistently showed a trend of an earlier thaw date across the pan-Arctic for the years 1988–2000, although the trend was only significant in North America (Table 5; Fig. 4a). During these same years, the trend in day of freeze was significant across the pan-arctic, with the day of freeze occurring $0.03 \, \text{days} \, \text{yr}^{-1}$ earlier according to the study by Smith *et al.* (2004), while TEM estimated a later day of freeze by $0.11 \, \text{days} \, \text{yr}^{-1}$ between 1988 and 2000 (Table 5; Fig. 4c), although the reasons for this discrepancy are not understood. The

Table 3 Comparison between TEM and NOAA snow cover chart data (Dye, 2002) incorporating only cells with available data for both data sets

Region (R)	Regional definition (grid cell means, 1972–2000)	Analysis	Area ($10^5 \, \text{km}^2$)	Percent of total area
Last observed snow cover in the spring (MLS)				
MLS-Jun	Weeks 22–26	D. Dye	3.24	20.51
	June	TEM	2.41	15.32
MLS-May	Weeks 17.5–22	D. Dye	4.10	25.89
	May	TEM	5.39	30.06
MLS-Apr	Weeks 13.5–17.5	D. Dye	4.97	31.43
	April	TEM	5.67	35.85
First observed snow cover in the fall (MFS)				
MFS-Sep	Weeks 36–39	D. Dye	1.14	7.23
	September	TEM	1.45	9.32
MFS-Oct	Weeks 39–43.5	D. Dye	5.85	37.00
	October	TEM	8.34	52.78
MFS-Nov	Weeks 43.5–47.5	D. Dye	7.18	45.41
	November	TEM	5.00	31.66
Duration of snow-free period ("weeks") (DSF)				
DSF-R1	Weeks 8–18	D. Dye	3.54	22.37
	Weeks 8–18	TEM	2.89	15.94
DSF-R2	Weeks 18–28	D. Dye	6.21	39.32
	Weeks 18–28	TEM	6.83	43.21
DSF-R3	Weeks 28–37	D. Dye	4.96	31.38
	Weeks 28–37	TEM	6.06	38.31

The total area includes all grid cells above 30°N. Therefore, the 'percent of total area' does not add up to 100% since not all cells fall into one of the three defined regions.
TEM, terrestrial ecosystem model.
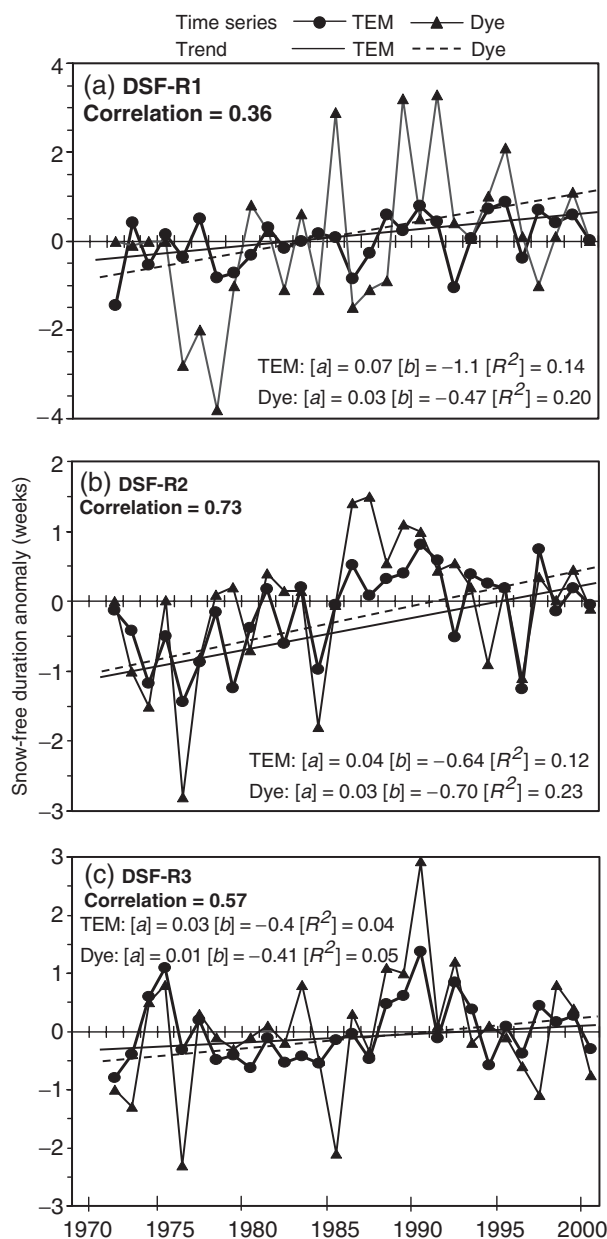
Fig. 3 Comparison of the trends (least-squares linear regression) in the duration of the snow-free period from 1972 to 2000 (anomaly in weeks) based on data from Dye (2002) and terrestrial ecosystem model (TEM). The duration of the snow-free (DSF) season in the DSF-R1 region (a) is 8.0–18.0 weeks, in the DSF-R2 region (b) the duration is 18.0–28.0 weeks, and the in DSF-R3 region (c) the duration is 28.0–37.0.

length of the growing season increase was statistically significant in North America, and both TEM and the study of Smith *et al.* (2004) found a shift in the growing season in Eurasia due to an earlier thaw and later freeze, although this was not statistically significant (Table 5; Fig. 4e).

In some regions, satellite-derived land-surface thaw data sets differ from each other as much as they differ from the TEM output. Across North America, the change in the day of thaw of -0.09 days yr^{-1} estimated by Smith *et al.* (2004) was in better agreement with that from TEM (-0.22 days yr^{-1}) than the estimate of -0.92 days yr^{-1} from that of McDonald *et al.* (2004). Differences across the three data sets illustrate the difficulties inherent in validating models with remotely sensed data due to varying processing algorithms in the remotely sensed data sets. Nevertheless, trends in greening and growing season length are consistently strong enough such that they cannot be merely explained as an artifact of the methods.

Based on our comparison of the permafrost map of Brown *et al.* (1998), the soil thermal model within TEM appears to appropriately capture the extent of the permafrost soils (Fig. 5a; Zhuang *et al.*, 2001). The TEM data showed permafrost in virtually every region where both continuous and discontinuous permafrost were depicted in the map of Brown *et al.* (1998; Fig. 5), with a slight difference in discontinuous permafrost found in southern Mongolia (Fig. 5b). Areas of isolated permafrost were not always evident in the data based on the TEM simulations, and some areas of sporadic permafrost southeast of the Hudson Bay in Canada were also not discernable in the data from the TEM simulations (Fig. 5b). In areas where the permafrost map as depicted by Brown *et al.* (1998) differs from that of the TEM permafrost map (Fig. 5), the spatial resolution of the model (0.5° latitude × 0.5° longitude) may be influencing the results, rather than the calculations of soil temperatures by the STM. It is likely that TEM does not capture some areas of sporadic and isolated permafrost because the data in the Brown *et al.* (1998) map are based on empirical ground measurements extrapolated from a smaller spatial scale (Heginbottom *et al.*, 1993).

Retrospective trends in C dynamics as related to changes in growing season length across MLS regions

Since we found the strongest trends in snow cover disappearance in the MLS regions (Table 4), we examined in more detail how decreases in snow cover might be related to area-weighted changes in soil freeze–thaw, growing season length, permafrost stability, and C dynamics across the MLS-Jun, MLS-May, and MLS-Apr regions (Table 6, with these trends represented with a 'Δ' symbol to differentiate between actual values). Although decreases in snow cover between 1960 and 2000 were greatest in the MLS-May region, permafrost degradation was greatest in the MLS-Apr region. In the MLS-Jun region, or those regions generally corresponding to extremely high latitudes (e.g. Fig. 2a),

Table 4 Trends in snow cover as simulated with TEM and for air temperature based on the input CRU data for regions north of 30°N during the years 1960–2000 using linear least-squares regression

Region (R)	Area (10^6 km^2)	Change in area (10^4 km^2 yr^{-1})	P-value	R^2	Change in T_{air} (°C yr^{-1})	P-value	R^2
MLS							
Jun	5.7	−2.5	0.0020	0.22	0.0304	<0.001	0.17
May	14.3	−5.4	<0.0001	0.38	0.0321	<0.001	0.35
Apr	16.0	−4.9	0.0060	0.18	0.0370	<0.001	0.27
Total	36.0	−12.8	—	—	—	—	—
MFS							
Sep	6.5	−1.2	0.1400	0.05	0.0198	<0.001	0.17
Oct	20.8	−4.5	0.0300	0.12	0.0255	<0.001	0.11
Nov	16.5	−0.9	0.3200	0.03	−0.0077	<0.001	0.01
Total	43.8	−6.6	—	—	—	—	—
DSF							
R1	7.4	−4.4	0.0003	0.29	—	—	—
R2	18.5	−5.2	0.0013	0.24	—	—	—
R3	17.1	−1.7	0.1100	0.10	—	—	—
Total	43.0	−11.3	—	—	—	—	—

'Change in T_{air}' refers to the change in air temperature based on the slope of the regression line and the defined month of first or last snow cover for each region. The snow cover regions are defined and depicted in Fig. 3. The duration of the snow free season in the DSF-R1 region is 8.0–18.0 weeks, in the DSF-R2 region the duration is 18.0–28.0 weeks, and the in DSF-R3 region the duration is 28.0–37.0.
TEM, terrestrial ecosystem model; MFS, month of first snow; MLS, month of last snow; DSF, duration of snow free.

the growing season length increased by 0.38 days yr^{-1} between 1960 and 2000, with increases being primarily due to earlier thaw. This lengthened growing season was greater than that in MLS-May or MLS-Apr regions, where the increase was ~ 0.20 days yr^{-1} between 1960 and 2000.

Although the MLS-Jun region showed the greatest increase in growing season length, the trends in NPP, R_h, and NEP were not as strong as the MLS-Apr and MLS-May regions between 1960 and 2000 (Table 6). The MLS-Apr region showed the greatest increases in NPP, and in the MLS-May and MLS-Apr regions, increases in R_h were more than double those of the MLS-Jun region (Table 6). The increases in R_h were less than the gains in NPP across all three MLS regions, and consequently, NEP showed a corresponding increase across all three regions (Table 6). Gains in NEP in the MLS-Apr region for the years 1960–2000 were similar to those in the MLS-May region due to higher values of R_h (Table 6). Nevertheless, despite these appreciable gains in NEP, the MLS-Jun and MLS-May regions may still act as a C source due to decreases in soil C that were not entirely counterbalanced by increases in vegetation C. That is, although the changes in NEP showed an increasing trend within these regions, the mean NEP (mean NEP = Δ Vegetation C−Δ Soil C; Table 6) could still be negative. These decreases in soil C were largest in both the MLS-May and MLS-Jun

regions, and smallest in the MLS-Apr region. Meanwhile, increases in vegetation C were largest in the MLS-Apr region and smallest in the MLS-Jun region (Table 6). This tradeoff between decreasing soil C and increasing vegetation C suggests that significant storage of C could switch between the soils and vegetation.

We performed linear regression analyses of area-weighted anomalies in growing season length to area-weighted anomalies in annual GPP, NPP, R_h, NEP, soil C storage and vegetation C storage across the three MLS regions (Fig. 6). Based on analysis over the years 1960–2000, we found that for each day that the length of the growing season increased, GPP increased by 18.2 g C m^{-2} yr^{-1} (note that GPP is not depicted in Fig. 6 since the trend was graphically similar to that of NPP), NPP by 9.1 g C m^{-2} yr^{-1}, R_h by 3.8 g C m^{-2} yr^{-1}, NEP by 5.3 g C m^{-2} yr^{-1}, and vegetation C by 8.9 g C m^{-2} 40 yr^{-1}. Soil C decreased by 8.1 g C m^{-2} 40 yr^{-1} for each day that the length of the growing season increased.

Comparisons of the baseline years (1976–2000) between the retrospective and prognostic simulations

Since we performed model simulations with two different spin-up periods depending on the time period of interest (e.g. 1960–2000 or 2001–2100), we evaluated the trends in thaw, freeze, growing season length,
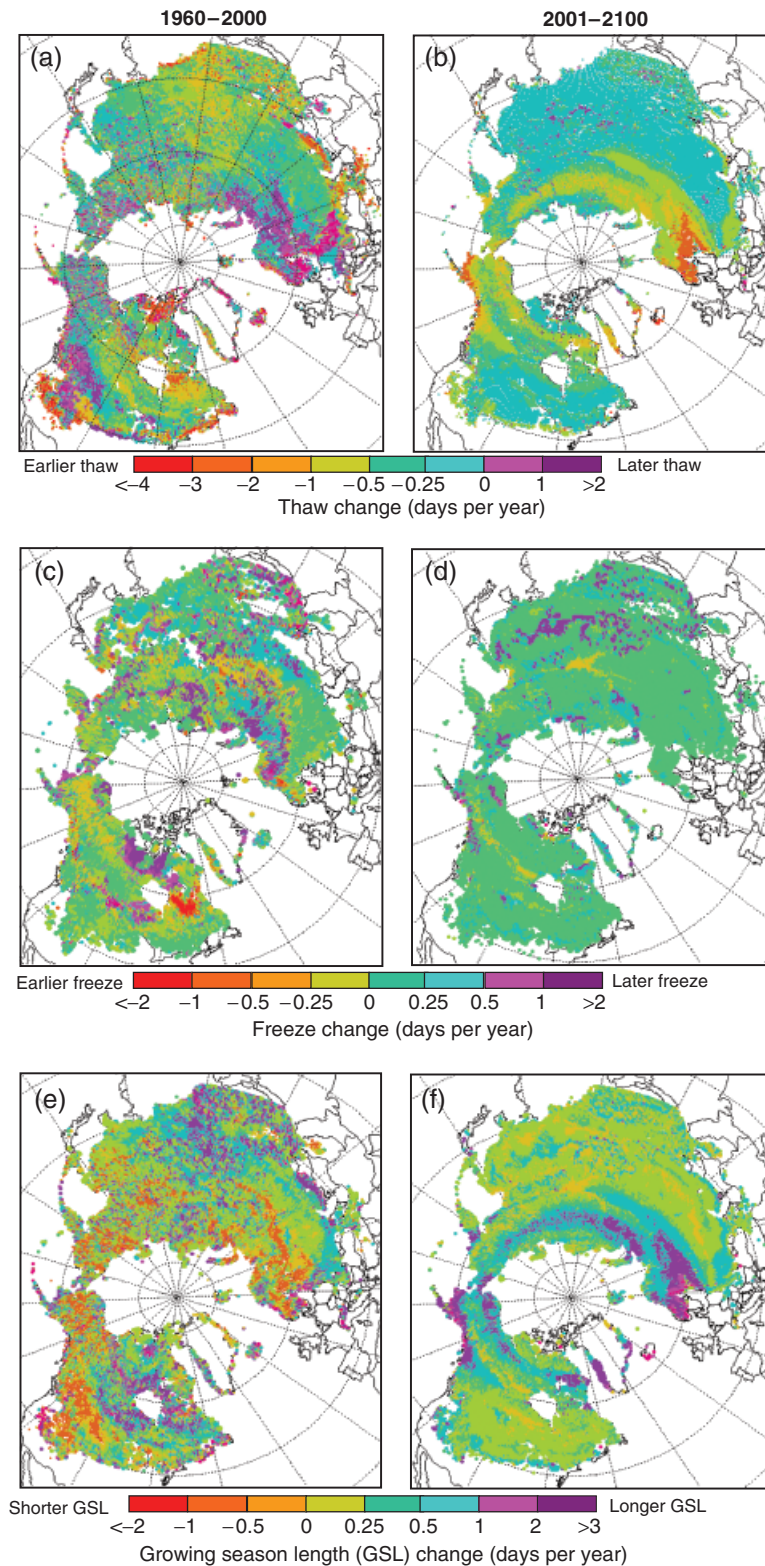
Fig. 4 Geographical depiction of trends in the day of thaw anomaly (a, b), day of freeze anomaly (c, d), and growing season length (GSL) anomaly (e, f) based on the slopes (days yr^{-1}) of linear regression analyses. The data depicted from the retrospective simulation is from the years 1988 to 2000 while that from the prognostic simulations is based on the years 2001–2100. The GSL is calculated as day of freeze minus day of thaw, such that the GSL is only depicted for areas with seasonal freezing and thawing of the soils.

Table 5 Comparison across three data sets for change in day of thaw and across two data sets for day of freeze and growing season length

Region	Study	Years	Change in anomalies (days yr^{-1})	R^2	P-value
Thaw					
Pan-Arctic	McDonald *et al.*		−0.43	0.34	0.02
	Smith *et al.*	1988−2000	−0.43	0.18	0.15
	TEM		−0.19	0.12	0.14
North America	McDonald *et al.*	1988−2000	−0.92	0.30	0.05
	Smith *et al.*		−0.09	0.29	0.06
	TEM		−0.22	0.19	0.08
Eurasia	McDonald *et al.*	1988−2000	−0.34	0.10	0.24
	Smith *et al.*		−0.36	0.14	0.20
	TEM		−0.15	0.01	0.30
Pan-Arctic			−0.36	0.96	<0.0001
North America	TEM	2001−2100	−0.42	0.96	<0.0001
Eurasia			−0.50	0.94	<0.0001
Freeze					
Pan-Arctic	Smith *et al.*	1988−2000	−0.03	0.00	0.08
	TEM		0.11	0.06	<0.0001
North America	Smith *et al.*	1988−2000	0.21	0.16	0.18
	TEM		0.26	0.08	0.36
Eurasia	Smith *et al.*	1988−2000	−0.29	0.02	0.62
	TEM		−0.31	0.12	0.18
Pan-Arctic			0.01	0.00	0.67
North America	TEM	2001−2100	−0.01	0.03	0.11
Eurasia			0.01	0.00	0.72
Growing season length					
Pan-Arctic	Smith *et al.*	1988−2000	0.46	0.35	0.03
	TEM		0.30	0.12	0.31
North America	Smith *et al.*	1988−2000	0.30	0.40	0.04
	TEM		0.48	0.20	0.03
Eurasia	Smith *et al.*	1988−2000	0.07	0.04	0.62
	TEM		0.16	0.10	0.36
Pan-Arctic			0.37	0.93	<0.0001
North America	TEM	2001−2100	0.41	0.91	<0.0001
Eurasia			0.51	0.91	<0.0001

The changes in the anomalies are based on slopes of linear regression analysis over the given regions.
TEM, terrestrial ecosystem model.

permafrost degradation, and C dynamics for the baseline years (1976–2000) for the prognostic simulation against those of the retrospective simulation based on the CRU data. The latitudinal band averaging for the 1976–2100 data set only slightly altered the trends in these dynamics for the region above 30°N during the baseline years of 1976–2000. The simulation based on the 1976–2100 data set indicated an earlier thaw by 0.26 days yr^{-1}, a later freeze by 0.09 days yr^{-1}, and an overall lengthening of the growing season by 0.35 days yr^{-1}. Meanwhile, the simulation based on the CRU data indicated an earlier thaw by 0.29 days yr^{-1}, a later freeze by 0.04 days yr^{-1}, and a lengthening of the growing season by 0.33 days yr^{-1} from 1976 to 2000.

During these same years, the loss in the area of stable permafrost was 5.4×10^4 km^2 yr^{-1} based on the simulation using the data set from 1976 to 2100 and 5.8×10^4 km^2 yr^{-1} based on the CRU data set.

In the simulation based on the interpolated 1976–2100 data set, GPP increased by 1.25 g C m^{-2} yr^{-1}, NPP increased by 0.45 g C m^2 yr^{-1}, R_h increased by 0.11 g C m^{-2} yr^{-1}, resulting in an increase in NEP by 0.34 g C m^{-2} yr^{-1} during the years 1976–2000. This resulted in a gain in vegetation C by 3.6 g C m^{-2} yr^{-1} and a loss of 3.2 g C m^{-2} yr^{-1} of soil C from 1976 to 2000. Meanwhile, during these same years, simulations based on the CRU data showed smaller increases in GPP (1.19 g C m^{-2} yr^{-1}), NPP (0.32 g C m^{-2} yr^{-1}), R_h (0.03 g C m^{-2} yr^{-1}),

Table 6 Trends, as represented by Δ, in snow cover area, permafrost stability, day of thaw, day of freeze, growing season length, GPP, NPP, R_h, NEP, vegetation C, and soil C for the three MLS snow cover regions for the years 1960–2000 and 2001–2100

Snow cover region	MLS-June	MLS-May	MLS-April
Total area for each region (10^6 km^2)	5.39	14.12	15.65
Percent of total area for each region	9%	34%	36%
Tundra	76%	38%	7%
Forest	23%	53%	66%
Vegetation type (%)			
Shrub/grass	1%	5%	23%
Other*	—	4%	4%
Years 1960–2000	Trend (*P*-value)		
Δ Snow cover area (km^2 yr^{-1})	-2.4×10^4 (0.003)	-5.3×10^4 (<0.0001)	-4.9×10^4 (0.007)
Δ Permafrost (km^2 yr^{-1})	-0.4×10^3 (0.162)	-8.8×10^3 (<0.001)	-32.9×10^3 (0.002)
Δ Thaw (days yr^{-1})	-0.36 (<0.001)	-0.19 (<0.001)	-0.19 (<0.0001)
Δ Freeze (days yr^{-1})	0.02 (0.785)	0.02 (0.539)	0.02 (0.668)
Δ Growing season length (days yr^{-1})	0.38 (<0.001)	0.21 (<0.0001)	0.20 (0.005)
Δ GPP (g C m^{-2} yr^{-1})	0.32 (0.001)	0.76 (<0.0001)	1.05 (<0.0001)
Δ NPP (g C m^{-2} yr^{-1})	0.17 (0.001)	0.39 (<0.0001)	0.52 (<0.0001)
Δ R_h (g C m^{-2} yr^{-1})	0.05 (0.002)	0.11 (<0.001)	0.23 (<0.0001)
Δ NEP (g C m^{-2} yr^{-1})	0.12 (0.020)	0.28 (<0.0001)	0.29 (<0.002)
Δ Vegetation C (g C m^{-2} yr^{-1})	0.4 (<0.0001)	3.0 (<0.0001)	7.6 (<0.0001)
Δ Soil C (g C m^{-2} yr^{-1})	-3.0 (<0.0001)	-3.6 (<0.0001)	-1.4 (<0.0001)
Mean NEP^2 (g C m^{-2} yr^{-1})	-2.6 (<0.0001)	-0.6 (<0.0001)	6.2 (<0.0001)
Years 2001–2100			
Δ Snow cover area (km^2 yr^{-1})	$-1.7\ 10^4$ (<0.0001)	$-5.7\ 10^4$ (<0.0001)	$-5.2\ 10^4$ (<0.0001)
Δ Permafrost (km^2 yr^{-1})	$-0.3\ 10^4$ (<0.0001)	$-3.3\ 10^4$ (<0.0001)	$-4.4\ 10^4$ (<0.0001)
Δ Thaw (days yr^{-1})	-0.45 (<0.0001)	-0.36 (<0.0001)	-0.38 (<0.0001)
Δ Freeze (days yr^{-1})	0.08 (<0.0001)	0.07 (<0.0001)	0.03 (0.0081)
Δ Growing season length (days yr^{-1})	0.53 (<0.0001)	0.43 (<0.0001)	0.41 (<0.0001)
Δ GPP (g C m^{-2} yr^{-1})	0.92 (<0.0001)	1.53 (<0.0001)	1.97 (<0.0001)
Δ NPP (g C m^{-2} yr^{-1})	0.32 (<0.0001)	0.61 (<0.0001)	1.03 (<0.0001)
Δ R_h (g C m^{-2} yr^{-1})	0.12 (<0.0001)	0.27 (<0.0001)	0.53 (<0.0001)
Δ NEP (g C m^{-2} yr^{-1})	0.20 (<0.0001)	0.34 (<0.0001)	0.50 (<0.0001)
Δ Vegetation C (g C m^{-2} yr^{-1})	2.1 (<0.0001)	8.6 (<0.0001)	22.0 (<0.0001)
Δ Soil C (g C m^{-2} yr^{-1})	0.1 (<0.0001)	-1.2 (0.0008)	-3.7 (<0.0001)
Mean NEP† (g C m^{-2} yr^{-1})	2.0 (<0.0001)	7.4 (0.0008)	18.3 (<0.0001)

The trends are based on the area-weighted slopes of linear regression analyses. Also show is mean NEP by area. The total area for each region takes into account all land areas above 30°N; 21% of the land area above 30°N did not fall into one of the three snow cover regions. Numbers in parentheses represent *P*-values.

*"Other" refers to small fractions of wetlands, savannas, or deserts.

†Mean NEP is calculated by subtracting Δ Vegetation C–Δ Soil C.

GPP, gross primary productivity; NPP, net primary productivity; R_h, heterotrophic respiration; NEP, net ecosystem productivity; C, carbon; MLS, month of last snow.

and NEP (0.29 g C m^{-2} yr^{-1}). The vegetation gained 3.2 g C m^{-2} yr^{-1} and the soils lost 2.8 g C m^{-2} yr^{-1}.

Future trends in snow cover, soil freeze–thaw, growing season length, permafrost, and C dynamics

Between the years 2001 and 2100, we found a continual earlier day of thaw, with Eurasia showing the strongest trend (0.50 days yr^{-1} earlier, Table 5, Fig. 4b). The trend

of earlier thaw was 0.36 days yr^{-1} across the pan-Arctic and 0.42 days yr^{-1} across North America. There was essentially no trend in day of freeze (Table 5; Fig. 4d), and consequently, the lengthening of the growing season was due entirely to an earlier day of thaw.

Across the MLS regions during the years 2001–2100 there were overall increases in growing season length, productivity and respiration (Table 6; Fig. 4f). As in the retrospective simulation, enhancements in NPP were
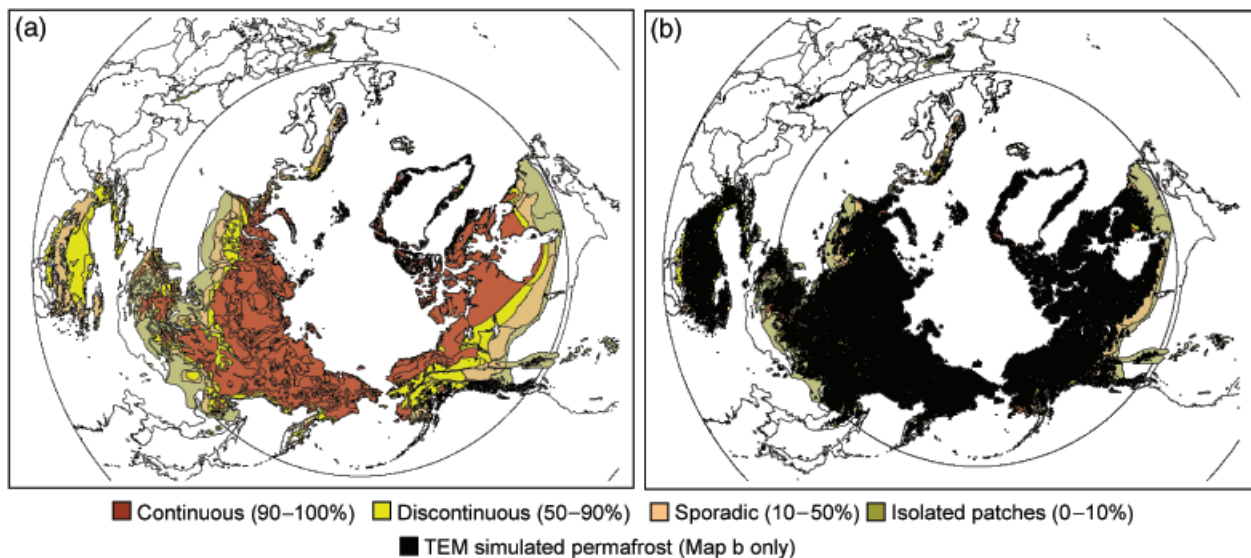
Fig. 5 Geographical extent of permafrost across the Circum-Arctic after Brown *et al*. (1998; map A), and terrestrial ecosystem model (TEM) simulations of permafrost overlain on the map of Brown *et al*. (1998; map B).

greater than those of R_h, translating to gains in NEP (Table 6). Gains in vegetation C were higher than losses of soil C across all three regions. Soil C decreased in the MLS-Apr and MLS-May regions, but showed a slight increase in the MLS-Jun region (Table 6).

For each day that the growing season increased across the MLS regions during the years 2001–2100, GPP increased by $37.1\,g\,C\,m^{-2}\,yr^{-1}$, NPP increased by $18.3\,g\,C\,m^{-2}\,yr^{-1}$, R_h increased by $8.8\,g\,C\,m^{-2}\,yr^{-1}$, NEP increased by $9.5\,g\,C\,m^{-2}\,yr^{-1}$, and vegetation C increased by $33.8\,g\,C\,m^{-2}\,100\,yr^{-1}$ (Fig. 6). Soil C decreased by $13.2\,g\,C\,m^{-2}\,100\,yr^{-1}$ when the growing season anomaly was between -28 and 5 days per century. However, when the growing season anomaly was between 5 and 20 days per century, soil C began to increase by $22.2\,g\,C\,m^{-2}\,yr^{-1}$, indicating a potential shift of C storage from the vegetation to the soils.

Cumulative NEP

In the 30–60°N region, results from the retrospective simulation showed little decadal variability between 1960 and 2000, with cumulative NEP ranging from $0.31\,Pg\,C\,yr^{-1}$ in the 1960s to $0.41\,Pg\,C\,yr^{-1}$ during the 1990s (Fig. 7a). The region between 60°N and 90°N acted as a weak source of C in the 1960s–1980s, and ultimately shifting to a weak sink during the 1990s (Fig. 7c; $P < 0.001$). The effects of increasing CO_2 and climate variability contributed to decadal variability in NEP in both the 30–60°N and 60–90°N regions during the years 2001–2100 (Fig. 7b, d). In the region between 30°N and 60°N, NEP was $0.08\,Pg\,C\,yr^{-1}$ in the 2000s,

and by the 2090s, the NEP in the region between 30°N and 60°N was $1.7\,Pg\,C\,yr^{-1}$ (Fig. 7b). In the 60–90°N region, there was also increasing NEP, although this trend was not as strong as that of the NEP for the 30–60°N region. NEP increased from $0.07\,Pg\,C\,yr^{-1}$ in the 2000s to $0.46\,Pg\,C\,yr^{-1}$ during the 2090s (Fig. 7d) in the 60–90°N region. Also in this region, the month of peak C loss shifted from May during the 1960s–2050s to April during the 2060s–2090s (Fig. 7b, d).

Discussion

This study used a large-scale TEM (ver. 5.1) to assess how modifications in snow cover and soil freeze–thaw due to climate change and increases in atmospheric CO_2 might affect growing season length and productivity over the years 1960–2100. Our study supports the conclusion that lengthening of the growing season will likely have a direct impact on both net C uptake and respiration within terrestrial ecosystems. The data sets we used to validate our findings, those of high-latitude snow dynamics (Dye, 2002), freeze–thaw (McDonald *et al*., 2004; Smith *et al*., 2004), and permafrost mapping (Brown *et al*., 1998), agreed with our results. More generally, our study concurred with evidence from eddy covariance-based studies (e.g. Goulden *et al*., 1996; Frolking, 1997; Black *et al*., 2000; Baldocchi *et al*., 2001) and other observational, modeling, and satellite-based studies (e.g. Randerson *et al*., 1999; Keyser *et al*., 2000; Myneni *et al*., 2001). In our discussion below we examine in more detail: (i) how well our model
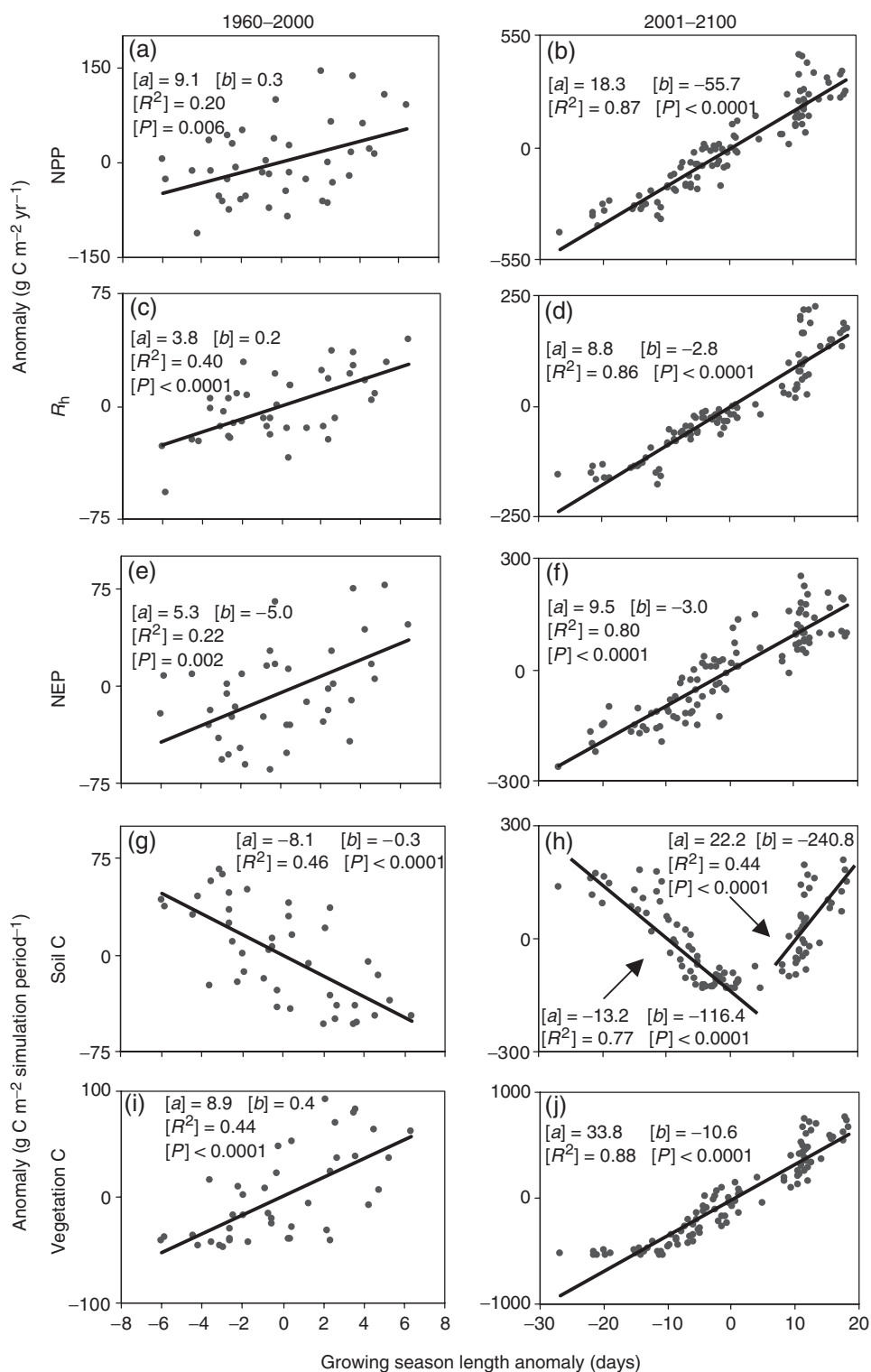
Fig. 6 Area-weighted anomalies of growing season length vs. anomalies in net primary productivity (NPP; a,b), heterotrophic respiration (R_h; c,d), net ecosystem productivity (NEP; e,f), soil carbon (Soil C; g,h), and vegetation carbon (Vegetation C; i,j) across the MLS-Apr, MLS-May, and MLS-Jun snow regions. The anomalies of the fluxes (NPP, R_h, and NEP) are given for each year, while the anomalies of the pools are given for each time period (e.g. 40 years for the retrospective simulation and 100 years for the prognostic simulation). Lines in each graph represent the linear least-squares regression, with [a] = slope, [b] = intercept, [R^2] = coefficient of determination, [p] = P-value. The trend in the anomaly of growing season length vs. the anomaly of gross primary productivity is graphically similar to that of NPP, but with different regression coefficients ([a] = 18.2; [b] = 0.7; R^2 = 0.28; $P < 0.001$ for the S2 simulation; and [a] = 37.1; [b] = −11.6; R^2 = 0.89; $P < 0.0001$ for the prognostic simulation).
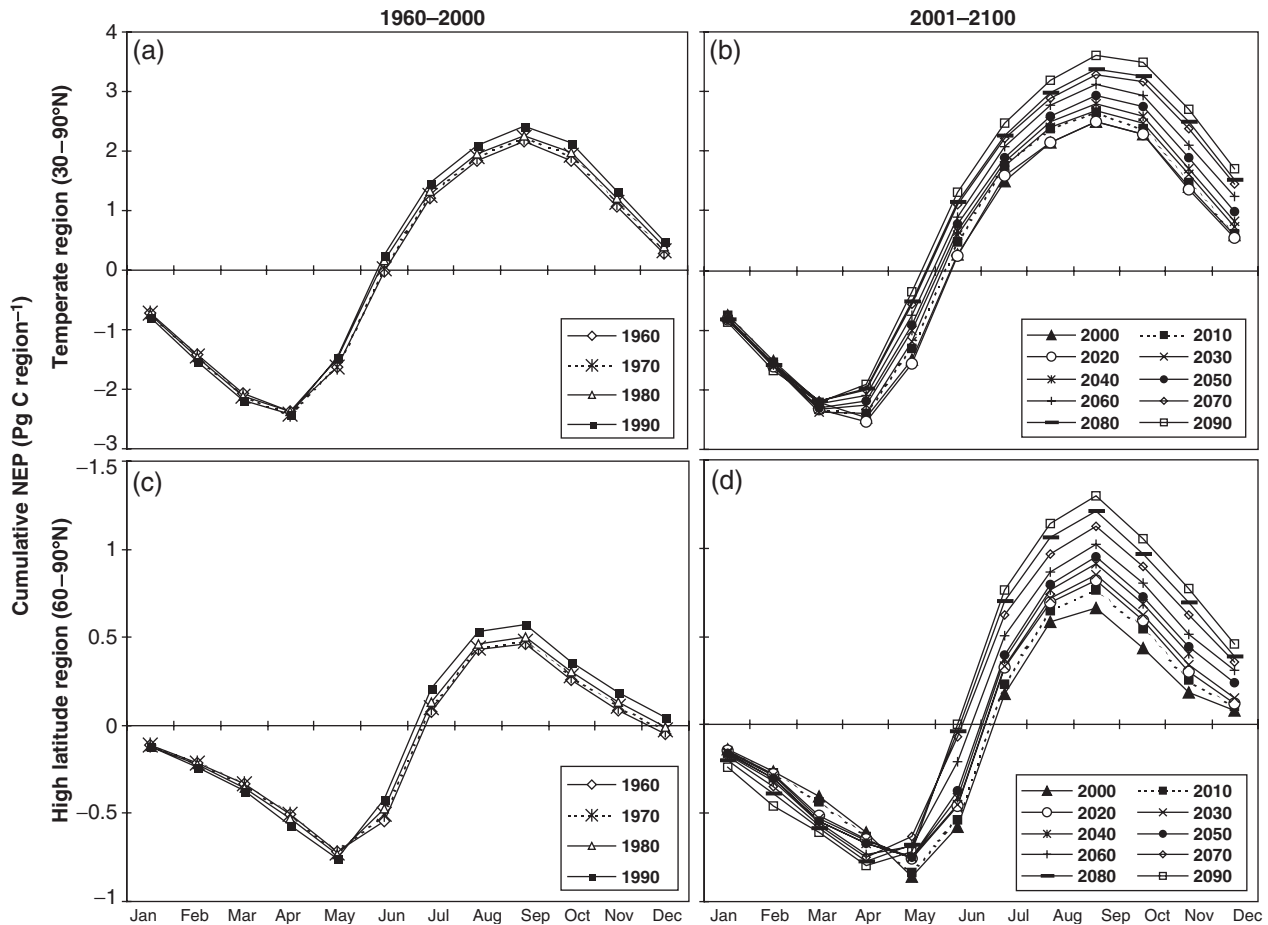
Fig. 7 Decadal variability in cumulative NCE from 1960 to 2100 for the regions 30–60°N (a–c) and 60–90°N (d–f).

simulations were suited for answering the three questions that we posed, (ii) how our results compare more generally to other studies that have examined these dynamics, and (iii) the potential importance of shifts in vegetation in relation to the findings from our study.

Overall evaluation of model simulations

Overall, the use of the TEM and the associated input data sets were an appropriate means by which to answer the three questions that we posed. Our analyses benefit from the explicit consideration of soil thermal dynamics in TEM. These dynamics influence the seasonality of C exchange in high-latitude ecosystems via the effects of freeze–thaw dynamics on C uptake and decomposition (Zhuang *et al.*, 2003). Future analyses based on TEM could benefit from explicitly considering the temperature control over heterotrophic respiration as it qualitatively changes across the freeze–thaw boundary (Michaelson & Ping, 2003), although empirical studies of this nature are still limited and the threshold is not yet determined.

While there are noticeable effects on productivity when changes in land-use are taken into account in the 30–60°N region, slight changes in agricultural land use in the 60–90°N region have a negligible effect on C storage at these latitudes in our simulations (Zhuang *et al.*, 2003). This finding suggests that in high latitudes enhanced C uptake in recent decades is due in large part to changes in soil thermal dynamics. Consequently, although we did not take into account changes in land-use in this study, we believe that in high-latitude regions, such changes would have had negligible effects on our findings.

Although there are other future global warming scenarios that might elicit a different response than the one prescribed in our study, we chose the 'reference scenario' from the IGSM because it lay in between 'high end' and 'low end' scenarios, thereby providing an estimate of 'average' future climate change (Webster *et al.*, 2003). In future studies, it may also prove beneficial to perform analyses based on the long-term greenhouse gas emission scenarios developed by the Intergovernmental Panel on Climate Change (IPCC, 2001). Nevertheless,

the results from our prognostic simulation suggest that it is important to monitor global climate change indicators (e.g. temperature, precipitation, cloudiness, atmospheric CO_2) to assess which path we are following.

Model results compared generally to other studies

Our model results generally concur with eddy covariance studies in high latitudes that have suggested a strong link between the timing of spring thaw, growing season length, and C balance (Frolking, 1997; Goulden et al., 1998; Black et al., 2000). Eddy covariance studies in temperate broadleaved forests show that for each additional day that the growing season is extended, net C uptake increases by $5.7\,\mathrm{g\,C\,m^{-2}\,yr^{-1}}$ (Baldocchi et al., 2001). This finding is similar to the TEM estimate of $5.3\,\mathrm{g\,C\,m^{-2}\,yr^{-1}}$ increase in net C uptake for each day that the growing season is extended across the tundra, mixed forests, and shrubs/grasses of the MLS snow cover regions (Fig. 6e; Table 6). In an analysis of trends in growing season length based on observational evidence and a leaf phenology model, Keyser et al. (2000) estimated that from the 1940s to 1990s across Alaska and north-western Canada the growing season had lengthened by 2.6 day per decade, with a range of 0.48–6.97 day per decade. In addition, Myneni et al. (1997) found that the growing season of high-latitude terrestrial ecosystems increased by 12 days during the years 1981–1991 from analyses with satellite data.

Analyses based on biogeochemical and atmospheric modeling suggest that increased photosynthesis at the start of the growing season and enhanced respiration from a large, labile pool of decomposing soil occurred in northern high latitudes between the years 1980 and 1997 (Randerson et al., 1999). These increased respiration rates may be offset by greater nutrient availability that promotes productivity (Bonan & Van Cleve, 1992; Oechel & Billings, 1992). Studies of forest inventory and satellite data identified biomass C gains in Eurasian boreal and North American temperate forests, with losses in some Canadian boreal forests between 1981 and 1999 (Myneni et al., 2001). These gains in productivity and vegetation C could be counter-balanced by further thawing of frozen soils associated with a warming and drying that decreases water tables, exposes organic peat, increases growing season respiration rates, and results in an increasingly unstable soil C pool (Oechel & Billings, 1992; Goulden et al., 1998). In addition, an extended growing season may increase the supply of labile C and promote winter respiration (Brooks et al., 2004). However, it is also possible that the soil heterotrophs may acclimate to warmer temperatures, lowering soil respiration over the long-term (Giardina & Ryan, 2000), and increasing net C uptake.

Our results suggest that increases in growing season length are likely to be greatest in areas with longer snow cover duration (Table 6). However, since these areas are characterized by vegetation of low productivity (e.g. tundra in MLS-Jun vs. forest in MLS-Apr; Table 5), increases in NPP, NEP, vegetation C, and R_h are not as large as regions with shorter snow cover duration, more vegetation, but less pronounced increases in growing season length. Furthermore, our findings show a reduction in soil C with increases in growing season length (Fig. 6g), with greatest losses in those areas with more vegetation (Table 6); these findings also indicate that this trend could reverse in the future (Fig. 6h).

Potential shifts in vegetation as related to growing season onset and productivity

The trends detected in this analysis are interesting to consider in the context of shifts in vegetation that are not explicitly accounted for in our model, but may become important regulators of C dynamics over decadal time scales in the future. Northern coniferous ecosystems could potentially shift to ecosystems with a greater component of mixed broadleaf–needleleaf trees. The importance of this shift is best understood in light of the photosynthetic activity of deciduous and coniferous species. Deciduous species begin photosynthesis following leaf-out and are characterized by a short, concentrated growing season. Coniferous species exhibit low rates photosynthesis for longer periods of time, with net C uptake in midsummer easily dominated by high rates of respiration (Griffis et al., 2003). Consequently, these shifts in vegetation could alter the surface energy budget and may also generate changes in the observed cycle of CO_2 (Chapin et al., 2000; Eugster et al., 2000). In addition, there may be a northern advance of the treeline in boreal regions (Keyser et al., 2000; Lloyd et al., 2003), and the conversion of arctic tundra to shrubland (Sturm et al., 2005). The increased abundance of shrubs may contribute to increases in snow depth due to the ability of the shrubs to trap snow and an associated decrease in sublimation. These increases in snow depth may cause warmer soil temperatures, increased activity of the soil microbes, and higher rates of soil CO_2 efflux (Sturm et al., 2005). To more fully understand the uncertainties associated with these vegetation shifts, models are being developed and refined to simultaneously predict vegetation distribution and the dynamics of C storage in high-latitudes (e.g. Epstein et al., 2001; Kaplan et al., 2003).

Conclusions

This study suggests that there are strong connections between decreases in snow cover, increases in perma-

frost degradation, earlier thaw, later freeze, and a lengthened growing season. These dynamics substantially influence changes in C fluxes, including enhanced respiration and productivity in our analyses. Such enhancements yield increases in vegetation C, but overall decreases in soil C. Although trends in growing season length increases are greater at higher latitudes, increases in productivity and respiration are not as large as those in lower latitudes. The implications of the responses by terrestrial ecosystems to climate change are substantial. Projected warming during the coming decades raises even more questions. A positive feedback between spring snow-cover disappearance and radiative balance can result in warmer spring air temperatures (Groisman *et al.*, 1994; Stone *et al.*, 2002). These warmer spring air temperatures will then likely exacerbate the continued early thaw and growing season onset, leading to further modifications in productivity and net C uptake. Even small changes in global temperatures could result in imbalanced responses in arctic and boreal regions, with feedbacks that may enhance such processes as photosynthesis and respiration. Our analyses imply that the relative strength of these feedbacks affect the future trajectory of C storage in high latitude regions. Therefore, it is important to improve our understanding of the relative responses of photosynthesis and respiration to changes in atmospheric CO_2 and climate.

References

Baldocchi D, Falge E, Lianhong G *et al.* (2001) FLUXNET: a new tool to study the temporal and spatial variability of ecosystem-scale carbon dioxide, water vapor, and energy flux densities. *Bulletin of the American Meteorological Society*, **82**, 2415–2434.

Black TA, Chen WJ, Barr AG *et al.* (2000) Increased carbon sequestration by a boreal deciduous forest in years with a warm spring. *Geophysical Research Letters*, **27**, 1271–1274.

Bonan GB, Van Cleve K (1992) Soil temperature, nitrogen mineralization, and carbon source-sink relationships in boreal forests. *Canadian Journal of Forest Research*, **22**, 629–639.

Brooks PD, McKnight D, Elder K (2004) Carbon limitation of soil respiration under winter snowpacks: potential feedbacks between growing season and winter carbon fluxes. *Global Change Biology*, **10**, 1–8.

Brown J, Ferrians Jr OJ, Heginbottom JA *et al.* (1998, revised February 2001) *Circum-Arctic Map of Permafrost and Ground Ice Conditions.* National Snow and Ice Data Center/World Data Center for Glaciology. Digital Media, Boulder, CO.

Chapin III FS, McGuire AD, Randerson JT *et al.* (2000) Arctic and boreal ecosystems of western North America as components of the climate system. *Global Change Biology*, **6**, S211–S223.

Chapman WL, Walsh JE (1993) Recent variations of sea ice and air temperatures in high latitudes. *Bulletin of the American Meteorological Society*, **74**, 33–47.

Clein JS, Kwiatkowski BL, McGuire AD *et al.* (2000) Modelling carbon responses of tundra ecosystems to historical and projected climate: a comparison of a plot- and global-scale ecosystem model to identify process-based uncertainties. *Global Change Biology*, **6**, S127–S140.

Clein JS, McGuire AD, Zhang X *et al.* (2002) The role of nitrogen dynamics in modeling historical and projected carbon balance of mature black spruce ecosystems across North America: comparisons with CO_2 fluxes measured in the Boreal Ecosystem Atmosphere Study (BOREAS). *Plant and Soil*, **242**, 15–32.

Dye DG (2002) Variability and trends in the annual snow-cover cycle in Northern Hemisphere land areas, 1972–2000. *Hydrological Processes*, **16**, 3065–3077.

Dye DG, Tucker CJ (2003) Seasonality and trends of snow-cover, vegetation index, and temperature in northern Eurasia. *Geophysical Research Letters*, **30**, 405, doi:10.1029/2002GLO16384.

Epstein HE, Chapin III FS, Walker MD *et al.* (2001) Analyzing the functional type concept in arctic plants using a dynamic vegetation model. *Oikos*, **95**, 239–252.

Eugster W, Rouse WR, Pielke Sr. RA *et al.* (2000) Land-atmosphere energy exchange in Arctic tundra and boreal forest: available data and feedbacks to climate. *Global Change Biology*, **6**, S84–115.

Food and Agriculture Organization/United Nations Educational. Scientific and Cultural Organization (FAO/UNESCO) [1974] *Soil Map of the World*, **Vol. I–X**. UNESCO, Paris.

Frolking F. (1997) Sensitivity of a spruce/moss boreal forest net ecosystem productivity to seasonal anomalies in weather. *Journal of Geophysical Research*, **102**, 29,053–29,064.

Giardina C, Ryan M (2000) Evidence that decomposition rates of organic carbon in mineral soil do not vary with temperature. *Nature*, **404**, 858–861.

Goodrich LE (1976) *A numerical model for assessing the influence of snow-cover on the ground thermal regime.* PhD thesis, McGill University, Montreal. Canada, 410 pp.

Goulden ML, Munger JW, Fan S-M *et al.* (1996) CO_2 exchange by a deciduous forest: response to interannual climate variability. *Science*, **271**, 1576–1578.

Goulden ML, Wofsy SC, Harden JW *et al.* (1998) Sensitivity of a boreal forest carbon balance to soil thaw. *Science*, **279**, 210–217.

Griffis TJ, Black TA, Morgenstern K *et al.* (2003) Ecophysiological controls on the carbon balance of three southern boreal forests. *Agricultural and Forest Meteorology*, **117**, 53–71.

Groisman PY, Karl TR, Knight RW (1994) Observed impact of snow cover on the heat balance and the rise of continental spring temperatures. *Science*, **263**, 198–200.

Hansen J, Ruedy R, Sato M et al. (2001) A closer look at United States and global surface temperature change. Journal of Geophysical Research, **106**, 23,947–23,963.

Heginbottom JA, Brown J, Melnikov ES et al. (1993) Circumarctic map of permafrost and ground ice conditions. In: Proceedings of the Sixth International Conference on Permafrost, Vol. 2, pp. 1132–1136. South China University Press, Wushan, Guangzhou, China. Revised December 1997. National Snow and Ice Data Center/World Data Center for Glaciology, Boulder, CO.

International Panel on Climate Change, (IPCC) (2001) Climate Change 2001: IPCC Third Assessment Report. Cambridge University Press, New York.

Kaplan JO, Bigelow NH, Bartlein PJ et al. (2003) Climate change and Arctic ecosystems II: modeling, paleodat-model comparisons, and future projections. Journal of Geophysical Research, **108**, 8171, doi:10.1029/2002JD002559.

Keeling CD, Chin JFS, Whorf TP (1996) Increased activity in northern vegetation inferred from atmospheric CO_2 measurements. Nature, **382**, 146–149.

Keeling CD, Whorf TP, Wahlen M et al. (1995) Interannual extremes in the rate of rise of atmospheric carbon dioxide since 1980. Nature, **375**, 666–670.

Keyser AR, Kimball JS, Nemani RR et al. (2000) Simulating the effects of climate change on the carbon balance of North American high latitude forests. Global Change Biology, **6**, 185–195.

Lloyd AH, Rupp TS, Fastie CL et al. (2003) Patterns and dynamics of treeline advance in the Seward Peninsula, Alaska. Journal of Geophysical Research, **108**, 8161, doi:10.1029/2001JD000852.

Mack MC, Schuur EAG, Bret-Harte MS et al. (2004) Ecosystem carbon storage in arctic tundra reduced by long-term nutrient fertilization. Nature, **431**, 440–443.

McDonald KC, Kimball JS, Njoku E et al. (2004) Variability in springtime thaw in the terrestrial high latitudes: monitoring a major control on the biospheric assimilation of atmospheric CO_2 with spaceborne microwave remote sensing. Earth Interactions, **8**, 1–23.

McGuire AD, Apps M, Beringer J et al. (2002) Environmental variation, vegetation distribution, carbon dynamics, and water/energy exchange in high latitudes. Journal of Vegetation Science, **13**, 301–314.

McGuire AD, Clein J, Melillo JM et al. (2000a) Modeling carbon responses of tundra ecosystems to historical and projected climate: the sensitivity of pan-arctic carbon storage to temporal and spatial variation in climate. Global Change Biology, **6**, S141–S159.

McGuire AD, Melillo JM, Joyce LA et al. (1992) Interactions between carbon and nitrogen dynamics in estimating net primary productivity for potential vegetation in North America. Global Biogeochemical Cycles, **6**, 101–124.

McGuire AD, Melillo JM, Randerson JT et al. (2000b) Modeling the effects of snowpack on heterotrophic respiration across northern temperate and high-latitude regions: comparisons with measurements of atmospheric carbon dioxide in high latitudes. Biogeochemistry, **48**, 91–114.

Melillo JM, McGuire AD, Kicklighter DW et al. (1993) Global climate change and terrestrial net primary production. Nature, **63**, 234–240.

Michaelson GJ, Ping CL (2003) Soil organic carbon and CO_2 respiration at subzero temperature in soils of arctic Alaska. Journal of Geophysical Research, **108**, 8164, doi:10.1029/2001JD000920.

Mitchell TD, Carter TR, Jones PD et al. (2004) A comprehensive set of high-resolution grids of monthly climate for Europe and the globe: the observed record (1901–2000) and 16 scenarios (2001–2100). Tyndall Centre for Climate Change Research Working Paper 55, University of East Anglia, Norwich, UK, July, 25pp.

Myneni RB, Dong J, Tucker CJ et al. (2001) A large carbon sink in the woody biomass of northern forests. Proceedings of the National Academy of Sciences, **98**, 14,784–14,789.

Myneni RB, Keeling CD, Tucker CJ et al. (1997) Increased plant growth in the northern high latitudes from 1981 to 1991. Nature, **386**, 698–702.

NCAR/Navy (1984) Global 10-Minute Elevation Data. Digital Tape Available through National Oceanic and Atmospheric Administration, National. Goephysics Data Center, Boulder, CO.

Oechel WC, Billings WD (1992) Effects of global change on the carbon balance of arctic plants and ecosystems. In: Arctic Ecosystems in a Changing Climate (ed. Chapin III FS), pp. 139–167. Academic Press, New York.

Osterkamp TE, Romanovsky VE (1999) Evidence for warming and thawing of discontinuous permafrost in Alaska. Permafrost and Periglacial Processes, **5**, 137–144.

Permafrost Subcommittee (1988) Glossary of permafrost and related ground ice terms. Technical Memorandum No. 142, National Research Council of Canada, p. 156.

Poutou E, Krinner G, Genthon C et al. (2004) Role of soil freezing in future boreal climate change. Climate Dynamics, **23**, 621–639.

Raich JW, Rastetter EB, Melillo JM et al. (1991) Potential net primary productivity in South America: application of a global model. Ecological Applications, **1**, 399–429.

Randerson JT, Field CB, Fung IY et al. (1999) Increases in early season ecosystem uptake explain recent changes in the seasonal cycle of atmospheric CO_2 at high northern latitudes. Geophysical Research Letters, **26**, 2765–2768.

Sazonova TS, Romanovsky VE, Walsh JE et al. (2004) Permafrost dynamics in the 20th and 21st centuries along the East Siberian Transect. Journal of Geophysical Research, **109**, DO1108, doi:10.1029/2003JD003680.

Serreze MC, Walsh JE, Chapin III FS et al. (2000) Observational evidence of recent change in the Northern high-latitude environment. Climatic Change, **46**, 159–207.

Smith NV, Saatchi SS, Randerson JT (2004) Trends in northern latitude soil freeze and thaw cycles from 1988–2002. Journal of Geophysical Research, **109**, D12101, doi:10,1029/2003JD004472.

Sokolov AP, Stone PH (1998) A flexible climate model for use in integrated assessments. Climate Dynamics, **14**, 291–303.

Stone RS, Dutton EG, Harris JM et al. (2002) Earlier spring snowmelt in northern Alaska as an indicator of climate change. Journal of Geophysical Research, **107**, D10, doi: 10,1029/2000JD000286.

Sturm M, Schimel J, Michaelson G et al. (2005) Winter biological processes could help convert Arctic tundra to shrubland. Bioscience, **55**, 17–26.

Tian H, Melillo JM, Kicklighter DW et al. (1999) The sensitivity of terrestrial carbon storage to historical climate variability and atmospheric CO_2 in the United States. Tellus, **51B**, 414–452.

Van Cleve K, Oechel WC, Hom JL (1990) Response of black spruce (*Picea mariana*) ecosystems to soil temperature modifications in interior Alaska. *Canadian Journal of Forest Research*, **20**, 1530–1535.

Vörösmarty CJ, Moore III BM, Grace AL *et al.* (1989) Continental scale models of water balance and fluvial transport: an application to South America. *Global Biogeochemical Cycles*, **3**, 241–265.

Webster M, Forest C, Reilly J *et al.* (2003) Uncertainty analysis of climage change and policy response. *Climatic Change*, **61**, 295–320.

Xiao X, Melillo JM, Kicklighter DW *et al.* (1997) Linking a global terrestrial biogeochemistry model with a 2-dimensional climate model: implications for the global carbon budget. *Tellus*, **49B**, 18–37.

Xiao X, Melillo JM, Kicklighter DW *et al.* (1998) Transient climate change and net ecosystem production of the terrestrial biosphere. *Global Biogeochemical Cycles*, **12**, 345–360.

Zhou L, Tucker CJ, Kaufmann RK *et al.* (2001) Variations in northern vegetation activity inferred from satellite data of vegetation index during 1981–1999. *Journal of Geophysical Research*, **106**, 20,069–20,083.

Zhuang Q, McGuire AD, Harden J *et al.* (2002) Modeling the soil thermal and carbon dynamics of a fire chronosequence in interior Alaska. *Journal of Geophysical Research*, **107**, 8147, doi:10.1029/2001JD001244.

Zhuang Q, McGuire AD, Melillo JM *et al.* (2003) Carbon cycling in the extratropical terrestrial ecosystems of the Northern Hemisphere: a modeling analysis of the influences of soil thermal dynamics. *Tellus*, **55B**, 751–776.

Zhuang Q, Melillo JM, Kicklighter DW *et al.* (2004) Methane fluxes between terrestrial ecosystems and the atmosphere at northern high latitudes during the past century: a retrospective analysis with a process-based biogeochemistry model. *Global Biogeochemical Cycles*, **18**, GB3010, doi:10.1029/2004GB002239.

Zhuang Q, Romanovsky VE, McGuire AD (2001) Incorporation of a permafrost model into a large-scale ecosystem model: evaluation of temporal and spatial issues in simulating soil thermal dynamics. *Journal of Geophysical Research*, **106**, 33649–33670.